

Supplementary Materials for

Theoretical Model of Substrate-Assisted Self-Assembly of DNA Nanostructures

Shogo Hamada^{*a} and Satoshi Murata^{*b}

^ahamada@molbot.mech.tohoku.ac.jp, shogo@nanoeng.net;

^bmurata@molbot.mech.tohoku.ac.jp

1	Calculation of DLVO energy between DNA and mica surface	1
1.1	Introduction to the Sushko's model	1
1.2	Calculation of Debye length	1
1.3	Van der Waals interactions between cylinder and surface	2
1.4	Double-layer forces between cylinder and surface	3
1.4.1	Outline of the calculation	3
1.4.2	Grahame equation	3
1.4.3	Poisson-Boltzmann equation	6
1.4.4	Pressure between cylinder and surface	6
1.5	Additional information about the calculation results	6
2	Rough estimation of monovalent/divalent cation concentrations in TAE/Mg²⁺ Buffer	8
2.1	Monovalent ion concentration	8
2.2	Divalent ion concentration	9
3	Calculation of ratio between 3-D and 2-D theoretical reaction rates	10
4	Theoretical speculation of adsorption model	11
5	Verification of activity parameter q	13
5.1	Obtaining parameter q	13
5.1.1	Experimental results (Initial conc. = 0.66 μ M)	13
5.1.2	Simulation results (Initial conc. = 0.66 μ M, $1/q = 6 \times 10^4$)	14
5.2	Verification of obtained parameter q	15
5.2.1	Additional experiments by spectrophotometer	15
5.2.2	Simulation results ($1/q = 6 \times 10^4$)	16
6	Additional figures of the simulation results	17
6.1	Free-solution self-assembly	17
6.2	Substrate-assisted self-assembly	18
6.2.1	Concentrations of species in the solution	18
6.2.2	Comparison of the contribution of ring formation on a surface	19
7	High-speed AFM observation	20

1 Calculation of DLVO energy between DNA and mica surface

1.1 Introduction to the Sushko's model

The interaction energy curve between DNA and mica surface is derived using DLVO (Derjaguin and Landau¹, Verwey and Overbeek²) theory. DLVO theory describes an interaction between two charged surfaces through liquid medium. The theory assumes that the interaction mainly comes from two types of forces: one is *van der Waals force*, and the other is *double-layer force*. Van der waals force is the sum of non-covalent and non-electrostatic interaction forces (London dispersion force, Debye force, etc.), even occur with neutral molecules. On the other hand, double layer force is occurred by a charged surface in a liquid. Surface charge is induced by dissociation of charged groups, or by adsorption of charged ions (or molecules) in solution. In case of mica-DNA, both surface is negatively like-charged, so the monovalent/divalent ion in solution (*i.e.* oppositely charged counterions) balances the surface charge. This counterion distribution gives the electric potential between two surfaces. Note that a “repulsive” force (not an attracting force) occurs between likely charged surfaces in counterion solution. This phenomenon is given by a osmotic pressure between counterions; an entropic effect surpasses a force rooted in electrostatic interactions³. Configurational entropy loss forces back the surfaces when both are approaching each other.

DLVO theory can be applied to any kind of shapes. In this section, we consider an interaction between a cylinder and a flat planar surface. Hereafter, a cylinder is considered as a model for DNA double helix and a planar surface is for mica surface.

Generic parameters and signs are given as follows (Fig. S1.1):

Distance between a cylinder and a planar surface d

Cylinder radius (DNA) $r_0 = 1[\text{nm}]$

Unit cylinder length $L = 0.34[\text{nm}]$ (Note that the calculation is based on the length of base pair.)

DLVO force curve can be written as a sum of van der Waals force ($vdW(d)$) and double layer force ($E_{dl}(d)$) as a function of distance d ,

$$DLVO(d) = vdW(d) + E_{dl}(d) \quad (\text{S1.1})$$

1.2 Calculation of Debye length

Van der Waals force and double-layer force between a cylinder and a plane both require the Debye length for its calculation. Debye length ($1/\kappa$) characterizes a screening/shielding distance of electric fields by ions in the solution⁴. The distance is affected by the concentrations and valence of ions; in case of buffer solution with several types of cations, we have to consider overall ionic strength of a solution.

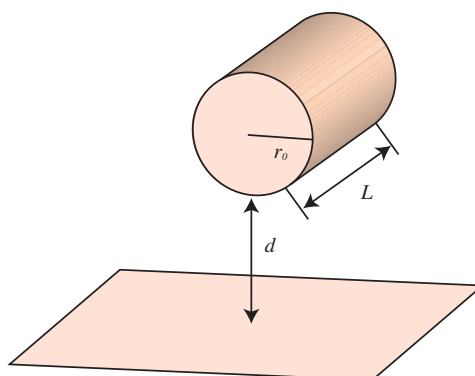


Figure S1.1: Signs used in DLVO model.

Ionic strength I of a solution is defined as,

$$I = \frac{1}{2} \sum_{n=i}^n c_i z_i^2 \quad (\text{S1.2})$$

where c_i is the molar concentration of ion i , z_i is the charge number of the ion. Concentration of each ion in case of TAE/Mg²⁺ 12.5mM buffer is calculated at Supplementary Materials Chapter 2.

Inverse square of the Debye length (κ^2) is defined as follows from a derivation of linearized Poisson–Boltzmann (Debye–Hückel) equation,

$$\kappa^2 = \frac{2e^2 I N_A}{D \epsilon_0 R T} \quad (\text{S1.3})$$

D is the dielectric constant of the solution. D is approximately equal to the dielectric constant of the solvent (in this case, water (≈ 78)), due to the small contribution of the ions themselves to the solution. N_A is Avogadro's number, e is elementary electric charge, ϵ_0 is permittivity of vacuum, R is gas constant, and T is temperature.

1.3 Van der Waals interactions between cylinder and surface

The calculation of non-retarded van der Waals force between a cylinder and a plane has been first investigated by Richmond⁵. Van der Waals force contribution at short distance ($\kappa d < 1$) is derived by Sushko⁶,

$$vdW(d) = -\frac{\pi r_0^2 L \kappa_m^2}{4d} (\Delta_{cm}^{\parallel} + \Delta_{cm}^{\perp} \cdot \Delta_{sm}^{\perp}) \quad (\text{S1.4})$$

The notations used in equation (S1.4) are:

$$\Delta_{cm}^{\parallel} = \frac{\epsilon_c^{\parallel} - \epsilon_m}{2\epsilon_m} \quad (\text{S1.5})$$

$$\Delta_{cm}^{\perp} = \frac{\epsilon_c^{\perp} - \epsilon_m}{\epsilon_c^{\perp} + \epsilon_m} \quad (\text{S1.6})$$

$$\Delta_{sm}^{\perp} = \frac{\epsilon_s^{\perp} - \epsilon_m}{\epsilon_s^{\perp} + \epsilon_m} \quad (\text{S1.7})$$

where ϵ_c^{\parallel} , ϵ_c^{\perp} are the dielectric permittivities of the cylinder in the parallel/perpendicular directions to the cylinder axis respectively, ϵ_s^{\perp} is the dielectric permittivity of the substrate, and ϵ_m is the dielectric permittivity of the medium. In case of DNA-Mica in aqueous solution, parameters are: $\epsilon_c^{\parallel} = \epsilon_c^{\perp} \approx 2.5$, $\epsilon_s^{\perp} \approx 5$ and $\epsilon_m \approx 78$.

κ_m^{-1} is a normalized Debye length⁷,

$$\kappa_m^2 = (\epsilon_0 k_B T) \kappa^2 \quad (\text{S1.8})$$

1.4 Double-layer forces between cylinder and surface

1.4.1 Outline of the calculation

Several steps are required to calculate double-layer forces between a cylinder and a surface (Fig. S1.2). Here we follow the steps proposed by Sushko⁷. First we calculate surface potential of both cylinder (DNA) and flat planar surface (Mica) using surface charge density of the materials. Second, the mid-plane potential (potential at the midpoint distance($d/2$) between DNA and mica) is derived by surface potential via Poisson-Boltzmann equation. Then the mid-plane pressure is calculated by summation of effect, arise from contributing ions in the solution. Finally, the pressure is integrated and the energy at the distance d is computed.

1.4.2 Grahame equation

Grahame equation gives a surface charge density of arbitrary material from surface potential of the material, monovalent/divalent cation concentration of solution, temperature etc. In this case, we inversely solve this equation in order to calculate the surface potential of cylinder (DNA) or plane (Mica) from surface charge densities.

Surface charge densities of DNA and mica can be calculated by physical properties and chemical formula of each material.

Mica A mica is a composite sheet in which a layer of octahedrally coordinated cations is sandwiched between two identical layers of linked (Si, Al)O₄ tetrahedra (Fig.S1.3)⁸. Calculated from the physical distance between oxygens exposed on a surface, a surface of mica has negative charges of $\sigma_{mica} = 2.1 \times 10^{18}$ sites/m² $\approx -0.3\text{C/m}^2$ ^{9,10}.

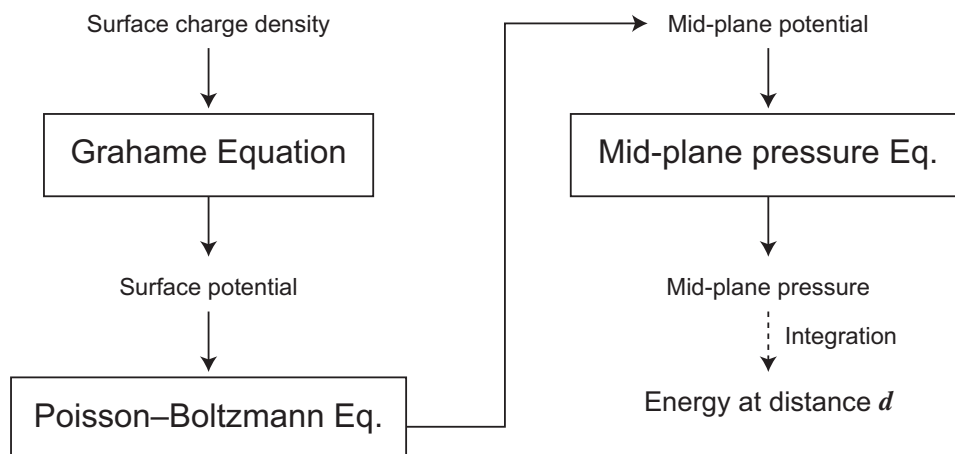


Figure S1.2: Outline of the double-layer force calculation.

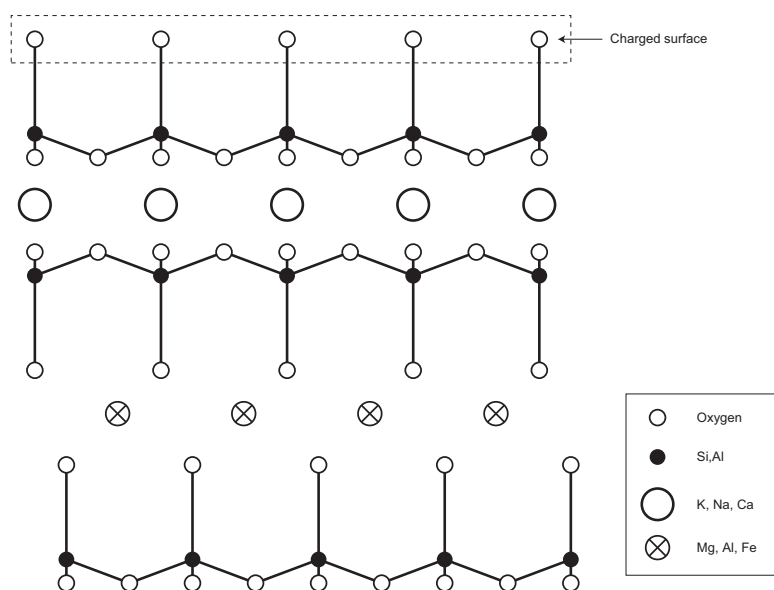


Figure S1.3: Cross section of the mica structure. Composite layers are linked by potassium ions. The surface of the mica is covered by hexagonally coordinated oxygens. The structure may be regarded as having a central layer $Mg_3(OH)_6$ (in phlogopite); *i.e.* each Oxygen exposed on a surface can be regarded as O^- .

DNA Consider DNA double helix as a cylinder. Each phosphate group in DNA backbone has one negative charged site, per strand. Therefore, surface charge density of the molecule is approximated as

$$\sigma_{DNA} = \frac{1}{(2\pi \cdot 0.34 \cdot 1/2) \times 10^{-18}} = 0.93 \times 10^{18} \text{sites/m}^2 \quad (\text{S1.9})$$

$$= -0.15 [\text{C/m}^2] \quad (\text{S1.10})$$

Grahame equation is written down as follows,

$$\sigma^2 = 2\epsilon_m \epsilon_0 k_B T \left\{ [\text{Na}^+]_{\infty} (e^{-e\psi_0^{pl,c}/k_B T} + e^{e\psi_0^{pl,c}/k_B T} - 2) + [\text{Mg}^{2+}]_{\infty} (e^{-2e\psi_0^{pl,c}/k_B T} + 2e^{e\psi_0^{pl,c}/k_B T} - 3) \right\} \quad (\text{S1.11})$$

Note that the equation can be used in any types of material if we can calculate surface charge density of the material. We do not have to restrict the counterpart of DNA adsorption to mica: we can also calculate other types of materials, such as silicon dioxide ($\sigma = -0.8 \text{C/m}^2$)¹¹, and can seek optimal ion concentration etc. for DNA binding.

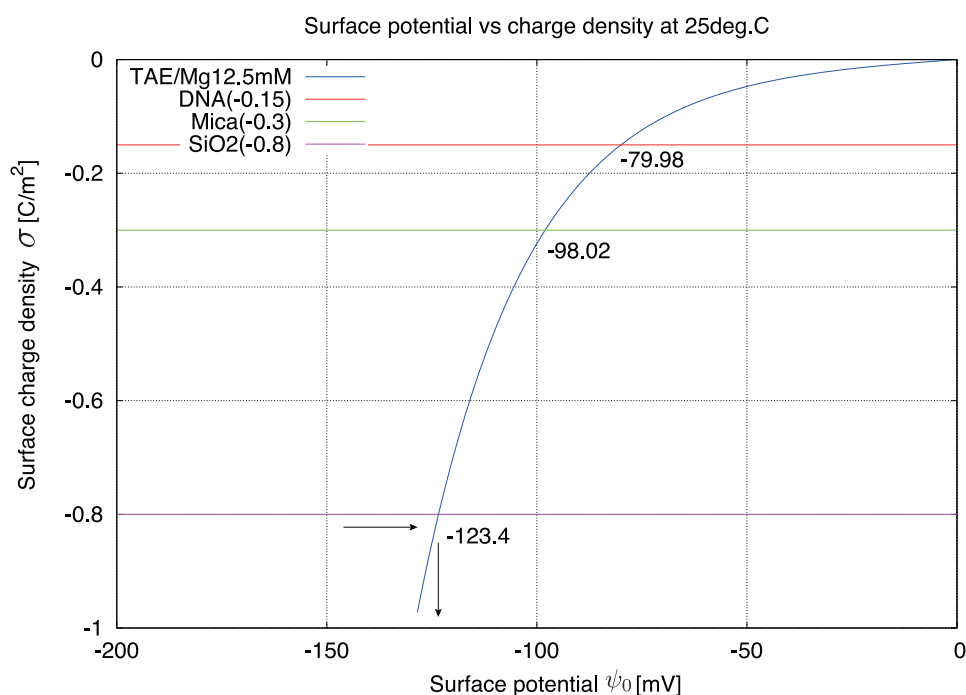


Figure S1.4: Results of Grahame equation of TAE/Mg²⁺ 12.5mM buffer at 25 °C.

Surface potential of DNA, mica and SiO₂ is calculated as an example (Fig. S1.4). Note that surface potential also depends on temperature T .

1.4.3 Poisson-Boltzmann equation

Mid-plane potential between two charged surfaces (ψ_m) are derived by a linear superposition approximation. This method calculates a potential at the mid-plane (distance $d/2$) between the cylinder and the flat plane surface using a sum of non-linear Poisson-Boltzmann equation¹².

$$\psi_{m,d/2} = \frac{2k_B T}{e} \left\{ \left(\ln \left[\frac{1 + \gamma_{pl}}{1 - \gamma_{pl}} \right] \right) + \left(\frac{K_0(\kappa(d/2 + r_0))}{K_0(\kappa r_0) \exp(-\kappa d/2)} \ln \left[\frac{1 + \gamma_c e^{-\kappa d/2}}{1 - \gamma_c e^{-\kappa d/2}} \right] \right) \right\} \quad (\text{S1.12})$$

γ_{pl} and γ_c are defined as

$$\gamma_{pl,c} = \tanh \left(\frac{e\psi_0^{pl,c}}{4k_B T} \right) \quad (\text{S1.13})$$

where K_0 is the zeroth-order modified Bessel function of a second kind,

$$K_0(x) = \int_0^\infty \frac{\cos(xt)}{\sqrt{t^2 + 1}} dt \quad (\text{S1.14})$$

1.4.4 Pressure between cylinder and surface

Using mid-plane potential (equation S1.12), the pressure between cylinder and planar surface is calculated as

$$P_x(d) = k_B T \rho_\infty(\text{NaCl}) [(e^{-e\psi_m/k_B T} - 1) + (e^{+e\psi_m/k_B T} - 1)] + k_B T \rho_\infty(\text{MgCl}_2) [(e^{-2e\psi_m/k_B T} - 1) + 2(e^{+e\psi_m/k_B T} - 1)] \quad (\text{S1.15})$$

where $\rho_\infty(\text{NaCl})$ and $\rho_\infty(\text{MgCl}_2)$ are the bulk concentration of salts, respectively. (The first term is the pressure contributed by Na^+ , the third term is contributed by Mg^{2+} , and the second and the fourth terms are contributed by Cl^- ions.)

Finally, the energy between cylinder and plane at distance d can be calculated as an integration of the pressure,

$$E_{dl}(d) = 2\pi r_0 L \int_d^\infty P_x(x) dx \quad (\text{S1.16})$$

1.5 Additional information about the calculation results

The obtained DLVO energy curve result has only one shallow minimum at 3.5[nm], -0.02[eV/bp]. Note that the interaction energy is given in unit of eV. The value is $\approx -0.92k_B T$ per base pair, when converted. This minimum value represents the energy of binding, and the distance is the preferable clearance between mica and DNA. Note that this distance is calculated

by using only two types of forces; other interactions, such as counterion correlated binding and various short-range effects are not considered, so the actual distance between mica and DNA might be different. However, when the DNA approaches far away from the surface (until around the debye length scale($\approx 1.69[\text{nm}]$)), this theory can be applied.

Another interesting result is that the scale of binding energy per base pair is about the same as $k_B T$. This suggests that, in TAE/Mg²⁺ buffer, binding of a single motif (assume ≤ 50 bp) still can be (weakly) fluctuated by a thermal motion.

2 Rough estimation of monovalent/divalent cation concentrations in TAE/Mg²⁺ Buffer

TAE buffer with Magnesium ion of 12.5mM concentration is one of the standard buffer we use in structural DNA nanotechnology. TAE stands for Tris base, Acetic acid and EDTA. In order to calculate adsorption energy on the mica surface, we have to solve the “actual” monovalent and divalent ion concentrations, because Tris/Tris-acetate is under equilibrium conditions.

A typical composition of TAE/Mg²⁺12.5mM buffer is as follows:

- Monovalent ion

Tris/Tris-acetate 40mM

- Divalent ion/ Chelating agent

EDTA (Ethylenediaminetetraacetic acid) 1mM

Mg²⁺ 12.5mM

- final pH: 8.3

2.1 Monovalent ion concentration

We assumed Tris-acetate acts as a monovalent ion ([TrisH⁺]):

Tris-acetate [(HOCH₂)₃C – NH₃⁽⁺⁾ · CH₃COO⁽⁻⁾]

Tris [(HOCH₂)₃C – NH₂]

Acetate CH₃COOH ⇌ [CH₃COO⁻][H⁺]

Equilibrium constants of Acetate and Tris can be defined as:

$$K_a = \frac{[\text{CH}_3\text{COO}^-][\text{H}^+]}{[\text{CH}_3\text{COOH}]} \quad (\text{S2.1})$$

$$K_b = \frac{[\text{Tris}][\text{H}^+]}{[\text{TrisH}^+]} = 10^{-8.06} \quad (\text{S2.2})$$

Note that the ionization degree of Acetate is low (mostly in [CH₃COOH]) in Formula S2.1. pH of K_b is at 25 °C.

Several equations can be derived from the conditions above:

$$[\text{Tris}] + [\text{TrisH}^+] = 0.04[\text{M}] \quad (\text{S2.3})$$

$$[\text{H}^+] = 10^{-8.3} \quad (\text{S2.4})$$

Substitute the conditions into Formula S2.2,

$$\frac{[\text{Tris}] \cdot 10^{-8.3}}{[\text{TrisH}^+]} = 10^{-8.06} \quad (\text{S2.5})$$

therefore,

$$[\text{Tris}] = 10^{0.24} \cdot [\text{TrisH}^+] \quad (\text{S2.6})$$

From Equations S2.3 and S2.6,

$$[\text{TrisH}^+] = \frac{0.04}{1 + 10^{0.24}} = 0.0146[\text{M}] \quad (\text{S2.7})$$

2.2 Divalent ion concentration

Because of the excess concentration of Mg^{2+} in the buffer, we can neglect the chelating effect of EDTA to the divalent metal ions in this case. Consequently, the divalent ion concentration is 12.5[mM].

3 Calculation of ratio between 3-D and 2-D theoretical reaction rates

In this section, a rough estimation for the calculation of the rate constant of particle that reacts under a confinement in two-dimensional surface is discussed. Discussions in the body text explained that the actual rate constant is much smaller than the calculated results, so the direct calculation of 2-D rate constant is rather meaningless in actual use. In this theory, a fraction of 2-D/3-D reaction rate constant is calculated, which supposedly be the same value even in the real condition. (A discussion about χ_3 of the adsorption rate constant in the next section suggests that we can assume this approximation is valid if the probability of success is mostly the same in 2-D and 3-D, and is multiplied to the theoretical calculation.)

In theory¹³, the rate constant of two types of particles (A, B) in 3-dimensional bulk solution can be expressed as,

$$k_{3D} = 4\pi D_3 R \quad (\text{S3.1})$$

which R is the sum of the particle radius ($r_A + r_B$, known as the encounter radius) and D_3 is the sum of diffusion coefficients ($D_A + D_B$).

On the other hand, the two-dimensional rate constant of reaction is modeled by circular disks¹⁴⁻¹⁶,

$$k_{2D} = \frac{2\pi D}{\ln(b/R) - c} \quad (\text{S3.2})$$

in which b is the half of the mean distance between two "targets", in this case motifs. c is the constant that is different depends on the model and assumptions. In this theory, we use $c = 0.231$ ¹⁶.

Therefore, the fraction of the rate constant between dimensions is,

$$\frac{k_{2D}}{k_{3D}} = \frac{1}{2R(\ln(b/R) - c)} \left(\frac{D_2}{D_3} \right) \quad (\text{S3.3})$$

We used $D_2 = 5 \times 10^{-13}$, $D_3 = 1.3 \times 10^{-10}$ ¹⁷, $R = 10^{-8}$ m, $b = 2R$ for an extreme case of the reaction. The value can be calculated as,

$$\frac{k_{2D}}{k_{3D}} \approx 4 \times 10^5 \quad (\text{S3.4})$$

Thus, the forward reaction rate constant at two-dimensional surface would be,

$$k_{f,2D} = k_f \cdot \frac{k_{2D}}{k_{3D}} \approx 2.4 \times 10^{11} \quad (\text{S3.5})$$

The estimated result gives significantly larger forward reaction rate constant in 2D in comparison with the value in 3D. This value is used in the simulations of the main text.

4 Theoretical speculation of adsorption model

Define the reaction rate of adsorption v_a as,

$$v_a = \mu_3 P_p P_a P_r \quad (\text{S4.1})$$

in which μ_3 is the number of molecules that collides to the surface from gas/solution phase, P_p is the probability of that the collision location is the adsorption site, P_a the probability of that the site is available for adsorption, and P_r is the probability of the success of adsorption.

Note that this definition and the theory are originally used for direct hybridization kinetics of oligonucleotide to the surface with probe DNAs¹⁷; however, we can follow the same or similar formula because of the generality of kinetics colliding to two-dimensional surface from the bulk solution remains.

The rate of collisions μ_3 between a bulk solution of concentration c_3 and a solid wall of *unit surface area* of Brownian particles is derived below^{17,18}.

$$\mu_3 = \frac{\langle v \rangle_3 c_3}{4} \quad (\text{S4.2})$$

where $\langle v \rangle_3$ is the instantaneous speed of the Brownian molecule (averaged over the Maxwellian distribution of speeds).

For Brownian motion the velocity is finite, defined as¹⁹,

$$\langle v \rangle_n = \zeta_n \sigma_n \quad (\text{S4.3})$$

in which σ_n is the frequency of collision, multiplied by the run between the collisions ζ_n (or the Brownian persistence distance²⁰).

The frequency of collisions can be related to the diffusion coefficient D_n ,

$$D_n = \frac{\zeta_n \sigma_n^2}{2n} \quad (\text{S4.4})$$

Thus, from equations (S4.2), (S4.3) and (S4.4),

$$\mu_3 = \frac{3D_3 c_3}{2\sigma_3} \quad (\text{S4.5})$$

P_p is defined as a fraction of adsorption site area A_{site} and an average area of the surface per adsorption site area $A_{surface}$,

$$P_p = \frac{A_{site}}{A_{surface}} \quad (\text{S4.6})$$

$$= \frac{A_{site}}{\frac{1}{([S^*] + [SP])N_A}} \quad (\text{S4.7})$$

where N_A is Avogadro's number.

P_a is considered as the "vacancy" of the site, so the parameter is defined as,

$$P_a = \frac{[S^*]}{[S^*] + [SP]} \quad (\text{S4.8})$$

P_r is the probability of the adsorption that depends on the reaction. The probability is unknown and arbitrary assigned as χ_n .

As a result, the adsorption rate of colloidal particles from the bulk solution to the surface per unit area can be written as,

$$v_{ad} = \frac{3D_3 A_{site} N_A P_r}{2\sigma_3} [S^*][P] \quad (\text{S4.9})$$

$$= k_{ad} [S^*][P] \quad (\text{S4.10})$$

Note that $c_3 = [P]$, and the rate is defined by per unit area. The expression corresponds to the reaction of Langmuir model in the main text, and also it suggests that the value of k_{ad} depends on three-dimensional diffusion. The theoretical forward adsorption rate constant k_{ad} can be calculated by solving the values in equation (S4.9), using a method by Chan²⁰. However, as we mentioned in the main text, the theoretical value only gives an upper limit, so we used same k_f in our paper for the realistic value. Also notice that $\chi_3 \leq 0.001$, used in receptor-ligand model on cell surface by Axelrod¹⁹ and also used in hybridization model by Chan²⁰, qualitatively supports that the decrease of value is required in order of magnitudes to fit k_{ad} into realistic range.

5 Verification of activity parameter q

5.1 Obtaining parameter q

5.1.1 Experimental results (Initial conc. = 0.66 μM)

The annealing/melting curve of the ring structure is observed by spectrophotometer (Fig.S5.1). The curves indicate two-step formation of the structure: inflection point at higher temperature indicates the formation of motifs, and lower one indicates the formation of the ring structure. The theoretical model discusses only formation of the rings, so our interest is the lower inflection point in this case. Also notice that no hysteresis is observed in the curves: this result suggests that no nucleation process is happening in this ring model (only “one-dimensional process” of self-assembly is occurring).

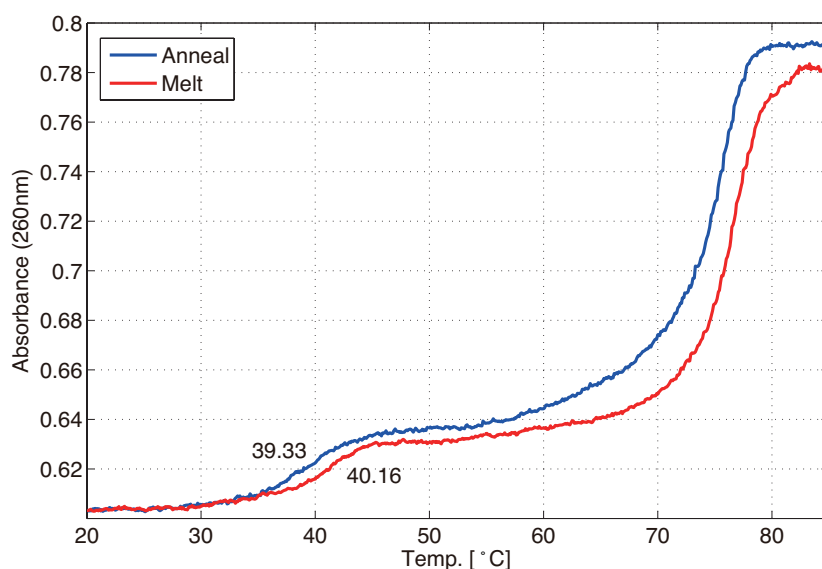


Figure S5.1: Experimental results of annealing and melting curve of T-motif Ring. Blue curve shows absorbance of 260nm during annealing (85 °C to 20 °C), and red curve shows the absorbance during melting (20 °C to 85 °C). Inflection point at lower temperature represents T_f (in case of annealing) and T_m (in case of melting).

5.1.2 Simulation results (Initial conc. = 0.66 μM , $1/q = 6 \times 10^4$)

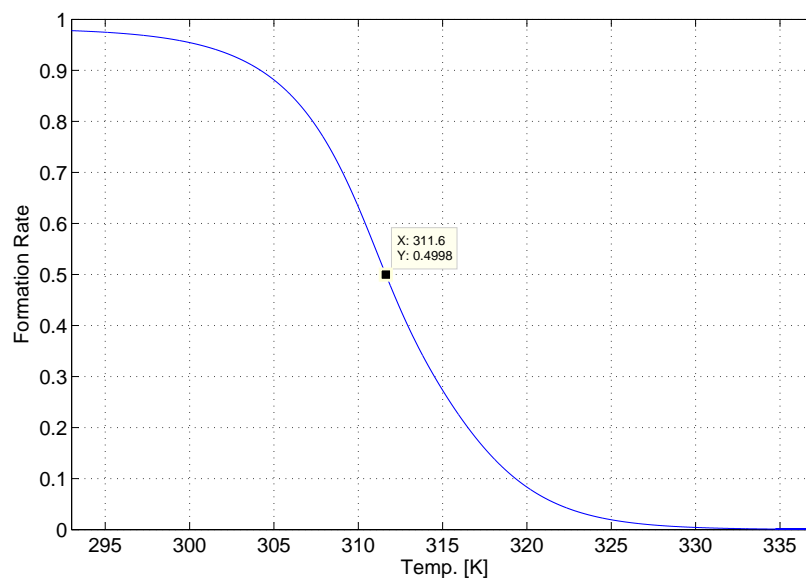


Figure S5.2: Formation rate (the ratio of hybridized sticky ends) versus temperature [K]. A temperature at formation rate= 0.5 is defined as T_f (formation temperature) of self-assembly. In this case, $T_f \approx 311.6[\text{K}]$. (Initial motif conc.=0.66 μM , $1/q = 6 \times 10^4$)

A formation rate (rate of hybridized sticky ends) of ring motifs in solution during the annealing process ($-0.3\text{ }^\circ\text{C}/\text{min.}$) is simulated by kinetic model (Fig.S5.2). The results show that although some non-hybridized sticky ends remain in solution, we have determined T_f from this graph.

5.2 Verification of obtained parameter q

5.2.1 Additional experiments by spectrophotometer

All experiments are carried out in free-solution environment (Fig.S5.3). Samples are prepared at $10\mu\text{M}$ (motif conc.) in TAE/ Mg^{2+} buffer. The sample is first annealed by hot water from 90°C to room temperature, and then diluted to the respective concentrations for measurements (10 , 1 , $0.5\mu\text{M}$). Measurements are done by heating up to 55°C , then cooling down to 20°C by the rate of $0.5^\circ\text{C}/\text{min}$. (Note that this measurement is focusing on the second process of formation curve (*i.e.* self-assembly of motifs).) UV wavelength is 260nm . V-630BIO (JASCO, Inc.) is used for measurement. Capillary jacket for melting temperature measurement is used for the experiment, so the exact volume of the sample is unknown. Calculated T_f (formation temperature) of respective samples are: 44.10°C [$10\mu\text{M}$], 38.37°C [$1\mu\text{M}$], 38.27°C [$0.5\mu\text{M}$]. $0.1\mu\text{M}$ was unable to measure because of the low concentration.

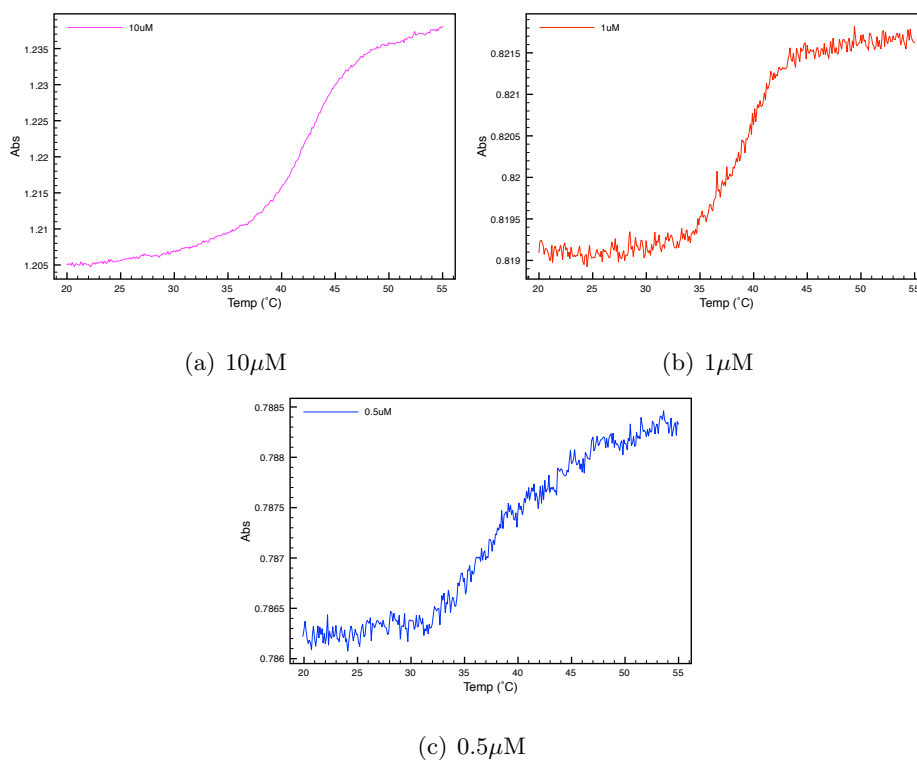


Figure S5.3: Formation curves of T-motif Ring 1.0x.

5.2.2 Simulation results ($1/q = 6 \times 10^4$)

Simulations are processed under same annealing rate of the real experiments ($-0.5 \text{ }^\circ\text{C}/\text{min}$) with respective motif concentrations (Fig.S5.4). The results using $1/q = 6 \times 10^4$ (TableS5.1) show that the simulated T_f qualitatively well agree with the experimental results. Note that this q value is optimized at $0.66 \text{ } \mu\text{M}$; the results show that errors become larger as the initial concentrations deviate from the original value.

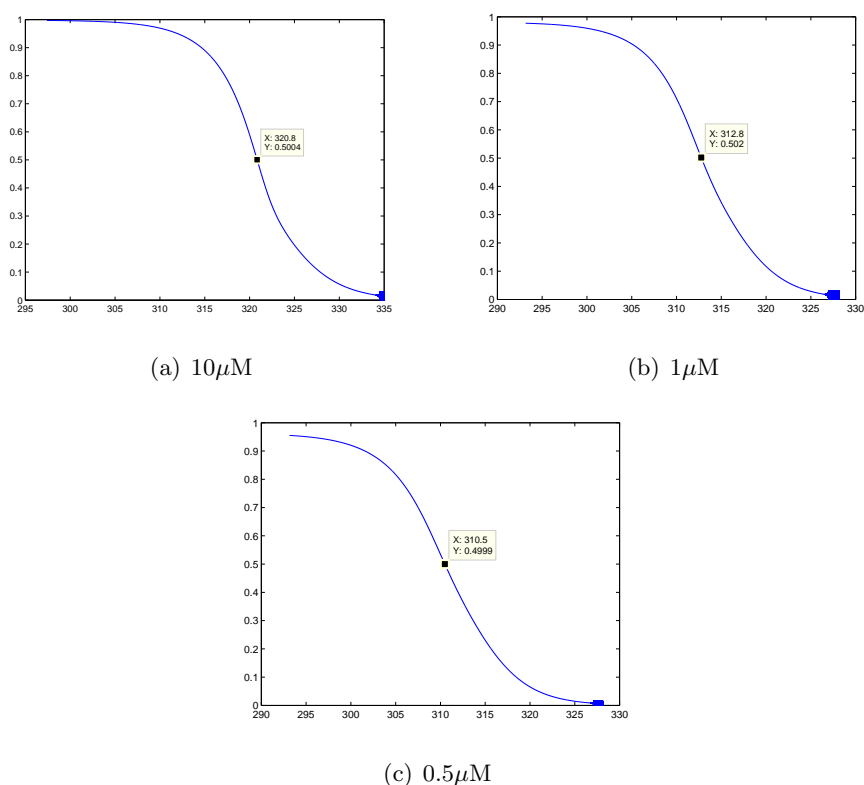


Figure S5.4: Simulation results (Formation rate) of T-motif Ring 1.0x.

Table S5.1: A comparison of the experimental and simulation results at $1/q = 6 \times 10^4$

Initial motif conc. (μM)	Experimental T_f [K]	Simulation T_f [K]
10	317.25	320.8
1	311.52	312.8
0.5	311.42	310.5

6 Additional figures of the simulation results

6.1 Free-solution self-assembly

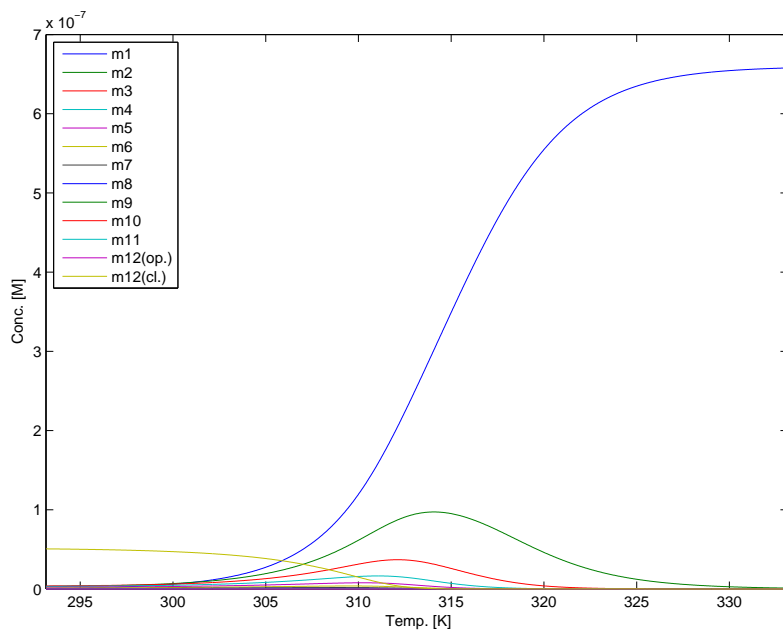


Figure S6.1: Concentration of the species (Initial motif conc.= $0.66 \mu\text{M}$, $1/q = 6 \times 10^4$).

Time-tracing of each species during the simulated annealing process ($-0.3 \text{ }^\circ\text{C}/\text{min.}$) is shown (Fig.S6.1). Note that $[m_{12}]$ increases and mostly dominates in the solution at the end of annealing.

6.2 Substrate-assisted self-assembly

6.2.1 Concentrations of species in the solution

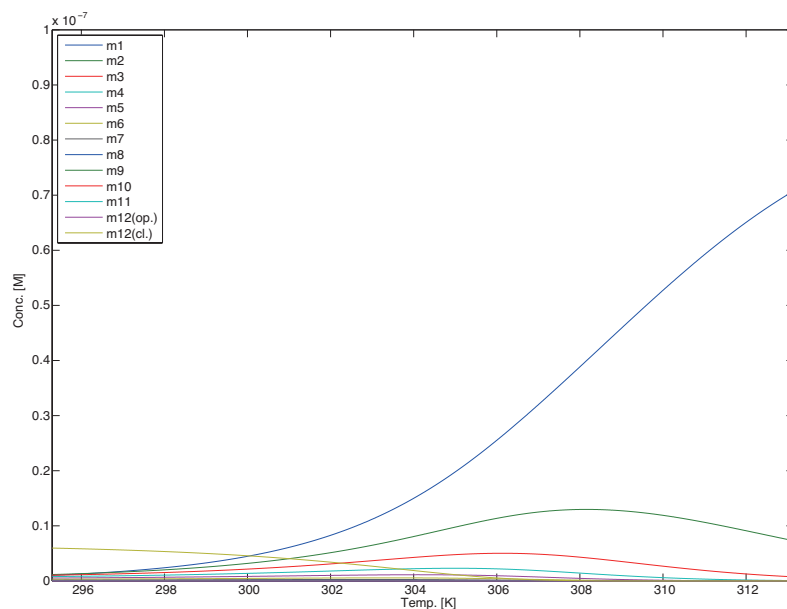


Figure S6.2: Concentration of the species in solution (Initial motif conc.= $0.1 \mu\text{M}$, $1/q = 6 \times 10^4$).

Fig. S6.2 shows the concentrations of the species in solution during annealing ($-0.05 \text{ }^\circ\text{C}/\text{min.}$), which is the counterpart of the result of the species on the substrate (Fig. 7 of the main text). Note that the trajectories of the species are mostly unchanged to the result of Fig.S6.1, because most of the motifs are still in solution and unaffected by the surface.

6.2.2 Comparison of the contribution of ring formation on a surface

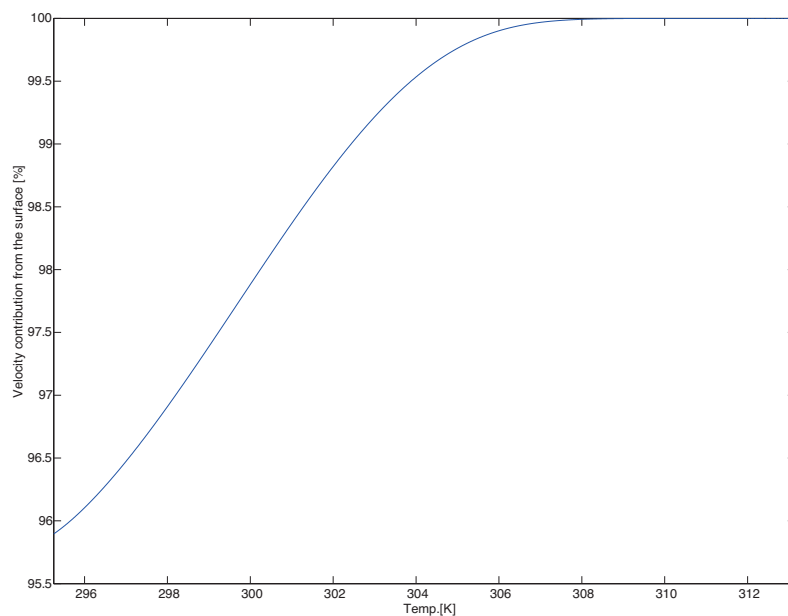


Figure S6.3: Percentage of formation rates of m12(close+open) contributed from self-assembly process.

The formation of rings on a surface via self-assembly and adsorption are compared by a calculation of a percentage of formation (Fig. S6.3). This shows that the most of the rings on a surface are supplied by self-assembly process; the difference of starting temperature of formation between in solution and on the surface can be explained by this result. (*i.e.* The contribution from the solution is small, so the formation of the rings on the surface is less affected by the adsorption process and the starting temperature will become different.)

7 High-speed AFM observation

AFM observations of the rings (Fig.4a) were carried out by using High-speed AFM (RIBM). Note that in case of Fig.4a, we used free-solution self-assembly for sample preparation. Samples were prepared by following procedures:

1. Prepare 1 μ M (motif conc.) Ring 1.0x samples (TAE/Mg²⁺ 12.5mM buffer) in 0.6ml test tube, and then anneal by using hot water in a styrofoam box
2. Dilute Annealed ring solution to 3nM
3. Deposit 2 μ l sample on freshly cleaved mica, and wait 8 minutes
4. Rinse the mica surface (two times) by observation buffer (Tris/Tris-HCl 20mM, Mg²⁺ 10mM)
5. Wait 12 hours
6. Add distilled water (2 μ l), and wait 20 minutes
7. Rinse the mica surface once again by observation buffer, and then start observation using High-speed AFM (liquid environment)

References

- [1] B. Derjaguin and L. Landau, *Acta Physico Chemica URSS*, 1941, **14**, 633.
- [2] E. J. W. Verwey and J. T. G. Overbeek, *Theory of the stability of lyophobic colloids*, Elsevier (Amsterdam), 1948.
- [3] J. Israelachvili, *Intermolecular and Surface Forces (Second Edition)*, Academic Press, 1992.
- [4] K. A. Dill and S. Bromberg, *Molecular Driving Forces*, Garland Science, 2003.
- [5] P. Richmond, *J. Chem. Soc., Faraday Trans. 2*, 1974, **70**, 229–239.
- [6] M. L. Sushko, *Personal communication*, 2010.
- [7] M. L. Sushko and A. Shluger, *Materials Science and Engineering C*, 2007, **27**, 1090–1095.
- [8] W. Deer, R. A. Howie and J. Zussman, *Longman*, 1966.
- [9] O. J. Rojas, M. Ernstsson, R. D. Neuman and P. M. Claesson, *Langmuir*, 2002, **18**, 1604–1612.
- [10] F. Carlsson, E. Hyltner, T. Arnebrant, M. Malmsten and P. Linse, *JOURNAL OF PHYSICAL CHEMISTRY B*, 2004, **108**, 9871–9881.
- [11] Y. Dong, S. V. Pappu, and Z. Xu, *Anal. Chem.*, 1998, **70**, 4730–4735.
- [12] R. Tuinier, *Journal of Colloid and Interface Science*, 2003, **258**, 45–49.
- [13] M. v. Smoluchowski, *Zeitschrift für physikalische Chemie (Phys. Chem. (Leipzig))*, 1917, **92**, 129–168.
- [14] G. Adam and M. Delbrück, *Structural Chemistry and Molecular Biology*, 1968, 198–215.
- [15] H. Berg and E. Purcell, *Biophysical Journal*, 1977, **20**, 193–219.
- [16] J. Keizer, *Acc. Chem. Res.*, 1985, **18**, 235–241.
- [17] D. Erickson, D. Li and U. J. Krull, *Analytical biochemistry*, 2003, **317**, 186–200.
- [18] F. Reif, *Fundamentals of statistical and thermal physics*, McGraw-Hill, 1965.
- [19] D. Axelrod and M. D. Wang, *Biophysical Journal*, 1994, **66**, 588–600.
- [20] V. Chan, D. Graves and S. McKenzie, *Biophysical Journal*, 1995, **69**, 2243–2255.